Supplementary Information

Design of Polyphosphate Inhibitors: A Molecular Dynamics Investigation on Polyethylene-Glycol-Linked Cationic Binding Groups

Amirhossein Mafi[1,2], Srinivas Abbina[3], Manu Thomas Kalathottukaren[3], James H. Morrissey[4], Charles Haynes[2,5], Jayachandran N Kizhakkedathu[1,3], Jim Pfaendtner[6], Keng C. Chou,[1*]

[1]Department of Chemistry, University of British Columbia, Vancouver, BC V6T 1Z1, Canada

[2]Department of Chemical and Biological Engineering, University of British Columbia, Vancouver, BC V6T 1Z3, Canada

[3] Centre for Blood Research, Department of Pathology and Laboratory Medicine, University of British Columbia, Vancouver, BC V6T 1Z3, Canada.

[4] Department of Biological Chemistry, University of Michigan, Ann Arbor, MI, USA.

[5]Michael Smith Laboratories, University of British Columbia, Vancouver, BC V6T 1Z3, Canada.

[6] Department of Chemical Engineering, University of Washington, Seattle, Washington 98195, United States

*Corresponding author e-mail: kcchou@chem.ubc.ca

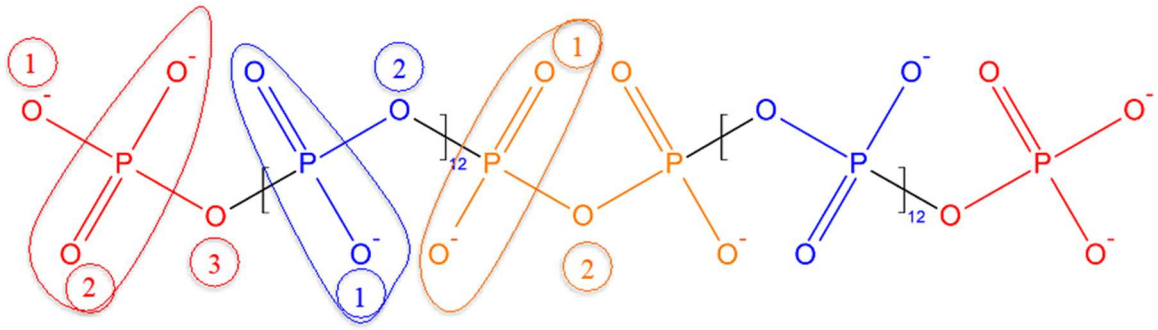

Figure S1. Molecular structure of polyphosphate (polyP). PolyP is divided into several identical groups on the basis of their structural symmetricity shown by different colors (red, blue, and orange), as described in Table S1. Each functional group is also divided into segments labeled with numbers.

Table S1. Calculated partial charges of atoms in polyP in the different groups and segments as indicated in Figure S1.

Atom	Charge	Segment	Atom	Charge	Segment	Atom	Charge	Segment
O^-	-0.889200	1	O^-	-0.886000	1	O^-	-0.886000	1
P	1.203300	2	P	1.443500	1	P	1.443500	1
O	-0.889200	2	O	-0.886000	1	O	-0.886000	1
O^-	-0.889200	2	O	-0.698400	2	O	-0.697400	2
O	-0.535700	3	-	-	-	-	-	-

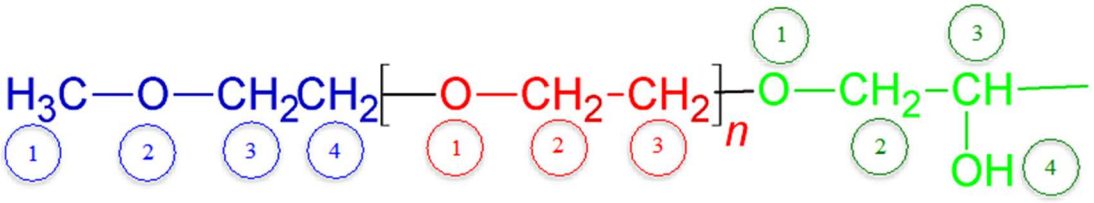

Figure S2. Molecular structure of the PEG-based tail. PEG is divided into three groups shown by red, blue, and green color as described in Table S2. Each group is then divided into segments labeled with numbers.

Table S2. Calculated partial charges of the PEG atoms in different groups and segments as indicated in Figure S2.

Atom	Charge	Segment	Atom	Charge	Segment	Atom	Charge	Segment
H	0.030300	1	O	-0.621300	1	O	-0.620200	1
H	0.030300	1	C	0.352400	2	C	0.387100	2
H	0.030300	1	H	-0.017500	2	H	-0.010700	2
C	0.127700	1	H	-0.017500	2	H	-0.010700	2
O	-0.454000	2	C	0.329500	3	C	0.268500	3
C	0.191200	3	H	-0.012800	3	H	-0.007800	3
H	0.012000	3	H	-0012800	3	O	-0.752500	4
H	0.012000	3	-	-	-	H	0.453100	4
C	0.361000	4	-	-	-	-	-	-
H	-0.023800	4	-	-	-	-	-	-
H	-0.023800	4	-	-	-	-	-	-

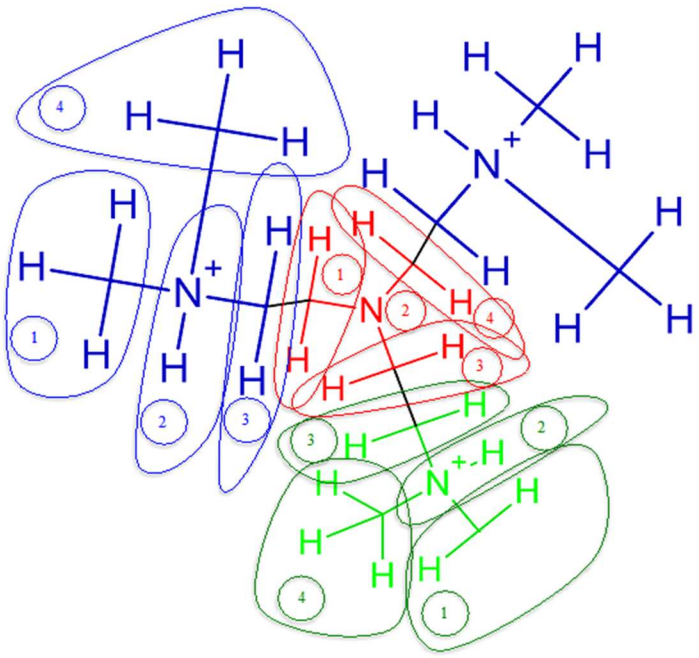

Figure S3. Molecular structure of the CBG R_1. R_1 is divided into the several identical groups on the basis of their structural symmetricity and shown in red, blue, and green as described in Table S3. Each group is then divided into segments labeled with numbers.

Table S3. Calculated partial charges of R_1 atoms in the different groups and segments as indicated in the Figure S3.

Atom	Charge	Segment	Atom	Charge	Segment	Atom	Charge	Segment
C	-0.312300	1	C	-0.123200	1	C	0.220300	1
H	0.189100	1	H	0.189100	1	H	0.049700	1
H	0.189100	1	H	0.189100	1	H	0.049700	1
H	0.189100	1	N^+	-0.025000	2	N	-0.514800	2
N^+	-0.025000	2	H	0.359200	2	C	0.220300	3
H	0.359300	2	C	-0.431900	3	H	0.049700	3
C	-0.431900	3	H	0.219700	3	H	0.049700	3
H	0.219700	3	H	0.219700	3	C	0.220300	4
H	0.219700	3	C	-0.312300	4	H	0.049700	4
C	-0.312300	4	H	0.189100	4	H	0.049700	4
H	0.189100	4	H	0.189100	4	-	-	-
H	0.189100	4	H	0.189100	4	-	-	-
H	0.189100	4	-	-	-	-	-	-

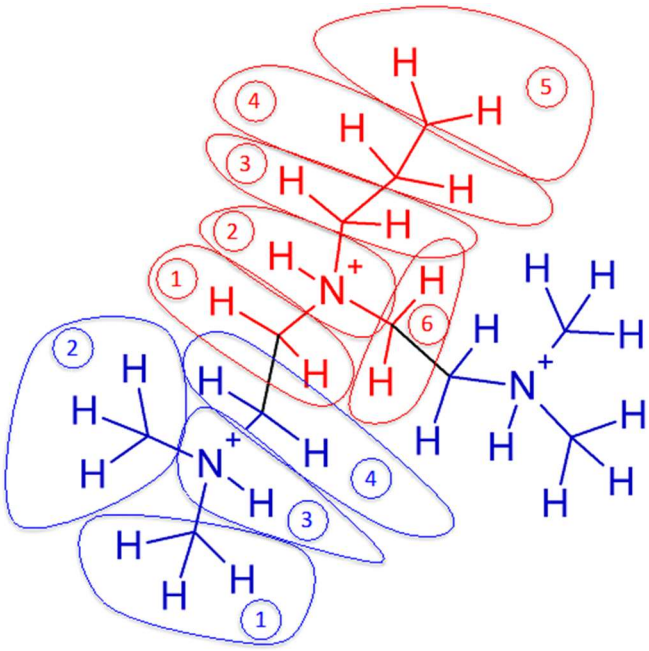

Figure S4. Molecular structure of the CBG R_2. R_2 is divided into the several identical groups on the basis of their structural symmetricity and shown in red, blue, and green as described in Table S4. Each group is then divided into segments labeled with numbers.

Table S4. Calculated partial charges of R_2 atoms in the different groups and segments as indicated in the Figure S4.

Atom	Charge	Segment	Atom	Charge	Segment
C	-0.004104	1	C	-0.316573	1
H	0.123293	1	H	0.202375	1
H	0.123293	1	H	0.202375	1
N^+	-0.060385	2	H	0.202375	1
H	0.318753	2	C	-0.316573	2
C	-0.181838	3	H	0.202375	2
H	0.155073	3	H	0.202375	2
H	0.155073	3	H	0.202375	2
C	0.010109	4	N^+	-0.056462	3
H	0.067558	4	H	0.378825	3
H	0.067558	4	C	-0.397737	4
C	-0.156478	5	H	0.222334	4
H	0.119408	5	H	0.222334	4
H	0.119408	5	-	-	-
C	-0.004104	6	-	-	-
H	0.123293	6	-	-	-
H	0.123293	6	-	-	-

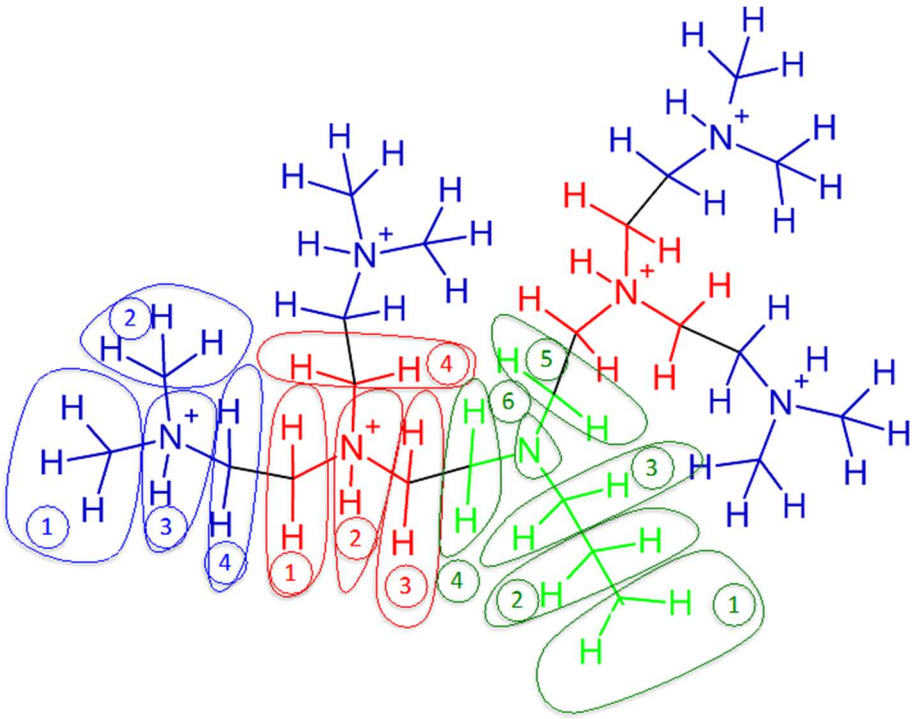

Figure S5. Molecular structure of the CBG R_3. R_3 is divided into the several identical groups on the basis of their structural symmetricity and shown in red, blue, and green as described in Table S5. Each group is then divided into segments labeled with numbers.

Table S5. Calculated partial charges of R_3 atoms in the different groups and segments as indicated in Figure S5.

Atom	Charge	Segment	Atom	Charge	Segment	Atom	Charge	Segment
C	-0.160925	1	C	-0.058773	1	C	-0.299274	1
H	0.103121	1	H	0.136969	1	H	0.203994	1
H	0.103121	1	H	0.136969	1	H	0.203994	1
C	0.051782	2	N^+	0.011677	2	H	0.203994	1
H	0.027503	2	H	0.338113	2	C	-0.299274	2
H	0.027503	2	C	-0.274243	3	H	0.203994	2
C	-0.216138	3	H	0.181743	3	H	0.203994	2
H	0.107176	3	H	0.181743	3	H	0.203994	2
H	0.107176	3	C	-0.058773	4	N^+	-0.062337	3
C	0.100094	4	H	0.136969	4	H	0.377527	3
H	0.060587	4	H	0.136969	4	C	-0.376338	4
H	0.060587	4	-	-	-	H	0.209086	4
C	0.100094	5	-	-	-	H	0.209086	4
H	0.060587	5	-	-	-	-	-	-
H	0.060587	5	-	-	-	-	-	-
N	-0.261342	6	-	-	-	-	-	-

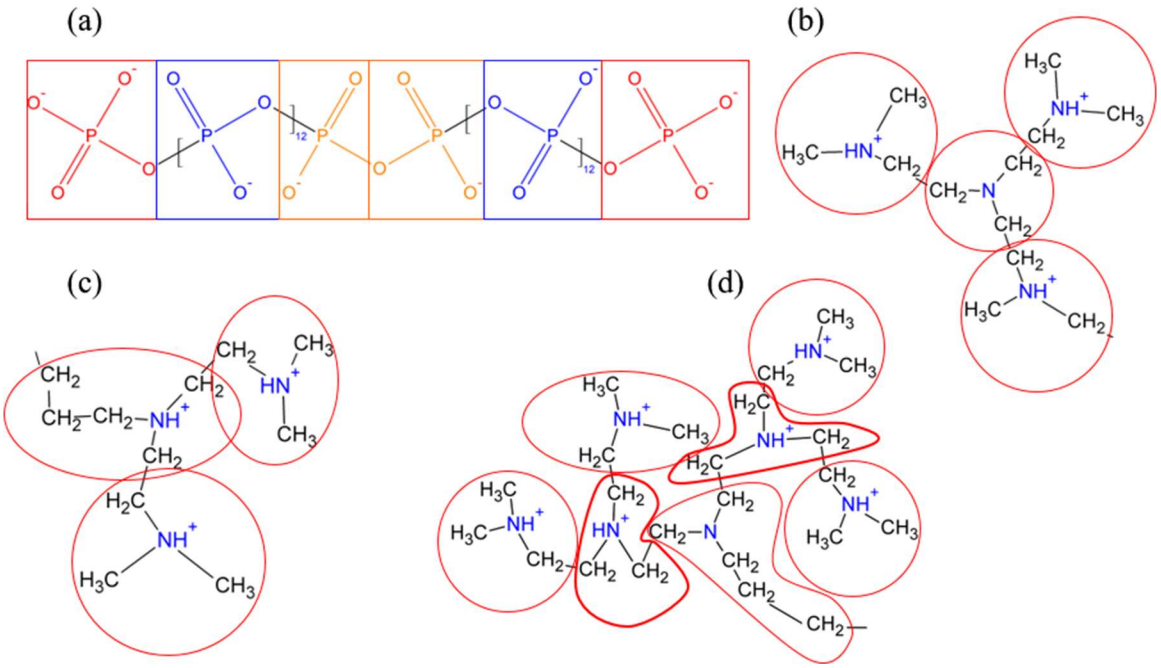

Figure S6. Definition of the coarse grained (CG) sites on (a) polyP, (b) R_1, (c) R_2, and (d) R_3 structure to calculate the Debye-Huckle (DH) energy based on eq. (2).

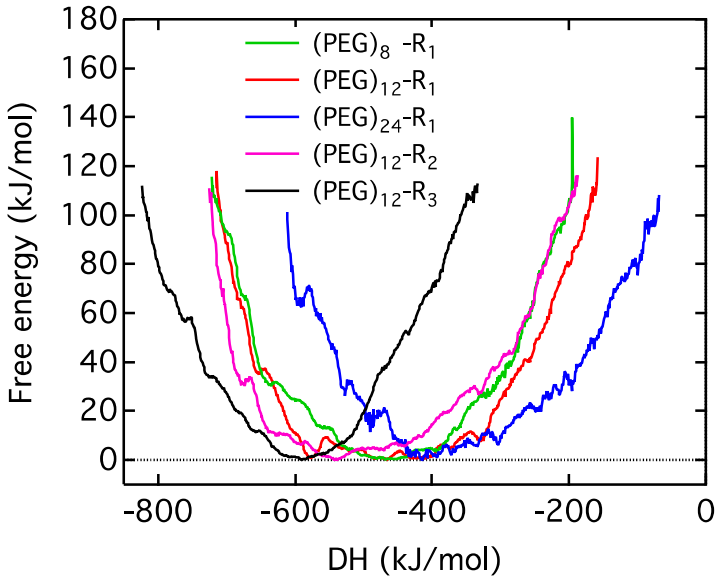

Figure S7. Free energy as a function of DH energy for the systems I to V.

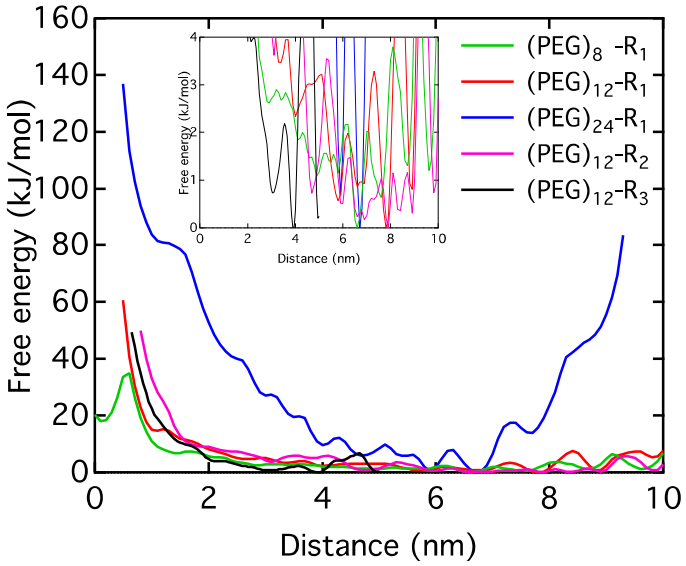

Figure S8. Free energy as a function of stoichiometry (S) number for the systems I to V.

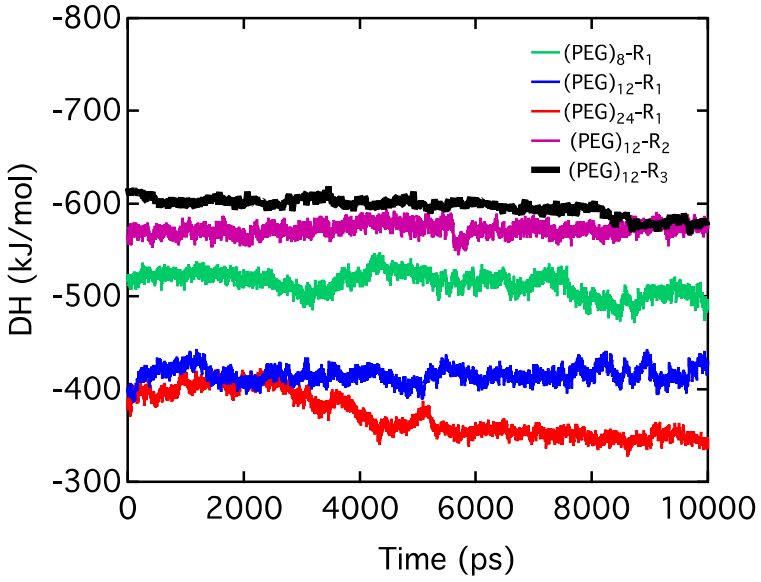

Figure S9. Examining the equilibration in terms of the Debye-Huckle (DH) energy according to the global free energy minimum of each system I to V as shown in Figure S7, after performing10 ns of regular molecular dynamics simulation in NPT ensemble.

Coarse grained force field development

To develop the coarse grained (CG) force fields for $(PEG)_{24}$-R_1 and PolyP, we followed the MARTINI[1] strategy, where every three or four heavy atoms are mapped into one bead. The all-atom (AA) to CG mapping of $(PEG)_{24}$-R_1 and PolyP are illustrated in Figure S10 and Figure S11, respectively. The coarse graining of the head group (R_1) and PolyP was done in a way that the symmetricity of the structures will not be disturbed. For this purpose, we had to choose 5:1 bead mapping in the initial and terminal phosphate (PO_4^-) groups and 3:1 bead mapping for the middle (PO_2^-) for the polyP.

The interactions between the beads are described using a combination of bonded potentials including bond stretching, angle bending, and torsions with different functional forms as presented in Table S6. To parameterize the bonded interactions, we performed a 200 ns MD simulation using the Generalized Amber force field (GAFF)[2] for the system I, in an NVT ensemble at the 310 K with the same procedure and conditions presented in the paper and Table 1. By coarse graining the $(PEG)_{24}$-R_1 and polyP in different trajectories in accord with the Figure S10-11, the bond, angle, and dihedral distributions were determined as illustrated in Figures S12-17. The same type of distributions can be obtained for the interactions between the CG particles by performing a 50 ns CG-MD simulation at 310K with the same procedure and conditions represented in the paper and Table 2. The parameters for the CG potentials were obtained by matching the bond, angle, and dihedral distributions resulted from the CG-MD simulation to the corresponding distributions from the AA-MD simulations. Table S6 represents the obtained parameters for describing the behavior of the drug and polyP, respectively. Note that, the CG parameters describing the

interactions in the PEG tail were borrowed from the Lee's work[2] with which they are able to predict the radius of gyration of PEG polymer accurately.

The non-bonded interactions are described using the Lennard-Jonnes and the Columbic potentials. The parameters of the non-bonded interactions are determined based on the chemical nature of the beads. Each bead in terms of the chemical nature are categorized into four major types of interaction sites: polar (P), non-polar (N), apolar (C), and charged (Q). To represent an accurate chemical nature of the underlying atomic structure, each particle type is divided into several subtypes in terms of capability of hydrogen bonding, and the degree of polarity.[1] The non-bonded parameters for each CG particle were adapted from "*martini_v2.2P.itp*"[3]. The adapted non-bonded parameters were designed to interact with the MARTINI polarized water model.[4] Table S7 represents the types of CG particles along with their charges used in this study.

To validate the developed CG force field, we calculated the binding free energy between $(PEG)_{24}$-R_1 and polyP and compared it to the one obtained from AA-MD simulation. The parallel tempering metadynamics in a well-tempered ensemble (PTMetaD-WTE)[5-8] was used to calculate the binding free energy. One polyP with 28 beads along with 10 CG $(PEG)_{24}$-R_1 were randomly inserted into the simulation box. The MARTINI polarizable water model (PW)[4] was used to describe the water behavior. In addition, 0.1 M of NaCl was also randomly placed into the solution. Before starting the dynamics, 30000 steps of the steep-descent energy minimization were performed to correct the positions of the beads. Then, a short 4-*ns* NPT simulation with a time step of 2 fs was performed to relax the CG particles. The dynamics were followed by running a 20 ns NPT simulation with a time step of 8 fs such that the temperature and pressure reached 310 K and 1 bar,

respectively. All dynamics were performed using the GROMACS 5.1.4 GPU computation algorithm[9-11]. The input options for implementing the simulations were mainly adapted from the "martini_v2.x_new.mdp"[12], with the following modifications. The neighbor list was updated every 40 steps. The temperature of the polyP/drugs/ions and water was separately maintained at 310 K using the V-rescale thermostat with a temperature constant of 0.3 ps.[13] The isotropic pressure coupling using Parrinello-Rahman barostat[14] with a pressure constant of 12.0 ps was used to maintain the system pressure at 1 bar with the compressibility of 3.0×10^{-4} bar^{-1}. The Lennard-Jones interactions were truncated at a cutoff radius of 1.1 nm. The potentials were modified by the potential-shift-Verlet. Periodic boundary conditions were applied to all three directions. The electrostatic interactions were treated by the reaction-field approach with a cutoff radius of 1.1 nm. The MARTINI polarizable water bonds were constrained using the P-LINCS algorithm[9] with a LINCS order of 4.

To start the PTMetad-WTE simulations, the last trajectory of the NPT simulation was chosen as an initial configuration of 6 different replicas at various temperatures, which were distributed exponentially[15] in the range of 310-460 K to achieve an efficient exchange rate between replicas. We performed a 10-ns MD simulation in the NVT ensemble so that each replica reached its specified temperature. Afterwards, a 20-ns well-tempered metadynamics simulation was carried out in a well-tempered ensemble[7, 16] to achieve an optimum exchange rate of 30-35% between the replicas. The bias factor of 60 was deposited with a Gaussian width of 250 KJ/mol, an initial Gaussian amplitude of 4.18 KJ/mol, and a deposition rate of 2 ps. The well-tempered metadynamics simulations were implemented using the PLUMED 2[17]. However, during the PTMetaD-WTE simulations,

the Gaussian was deposited every 240 ps. The Debye-Huckel (DH) energy[18] (eq. (1)) between the phosphate beads of polyP and the charged beads of R_1 was actively biased during the production run with a salt ionic strength of 0.1 M and water relative dielectric constant of 75 in order to compare with the DH energy obtained from the AA-MD simulations.

In addition, the drug binding stoichiometry (S) (see eq. (2)) number around polyP was also biased during the PTMetaD-WTE with the tuning parameters of n, m, and r_0 equal to 12, 24, and 1.5 nm, respectively. The bias factor for all systems was 20. The Gaussian bias was deposited every 1.6 ps with an initial amplitude of 2 KJ/mol, and a width of 0.2 KJ/mol. The PTMetaD-WTE simulation was performed for 4 μ using the PLUMED 2[17]. At the end, since the DH energy profile was less informative about the binding free energy, we implemented the reweighting[19] algorithm on the resulted PTMetaD-WTE trajectories to calculate the binding free energy of the drug to the polyP. Figure S18 and S19 show that variation of the free energy with the DH energy and the S number are fairly comparable to those calculated from the AA-MD simulation. The reweighted binding free energies between $(PEG)_{24}$-R_1 and polyP obtained from the GAFF and MARTINI force field are in good agreement with each other, as indicated in Figure S20.

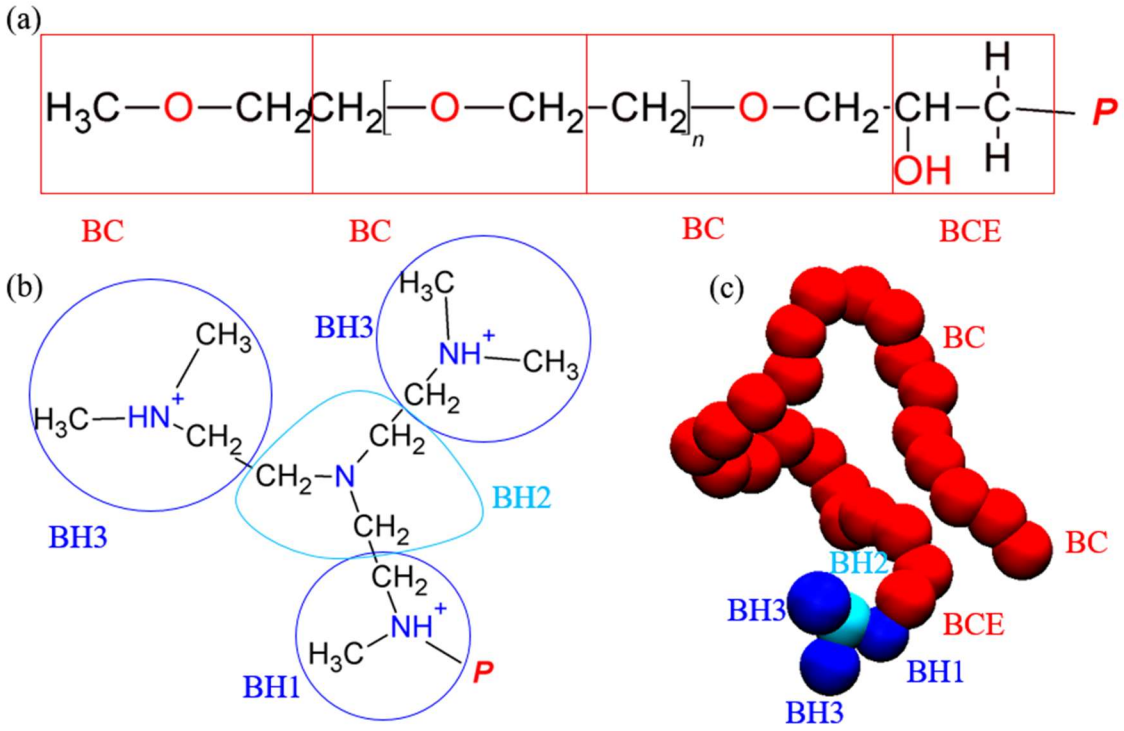

Figure S10. The MARTINI CG sites and their labeling for (a) PEG and (b) R_1. The *P* denotes the attachment location of PEG-based tail and the head group. (c) The CG structure of $(PEG)_{24}$-R_1.

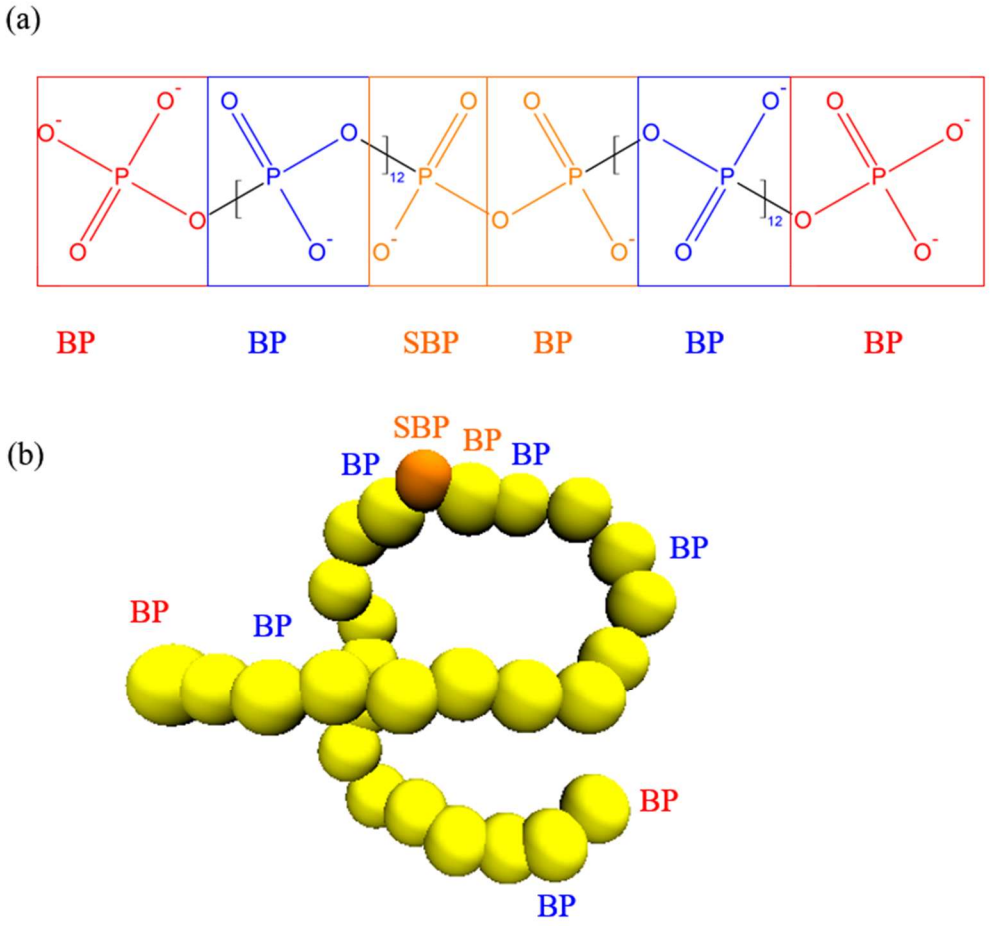

Figure S11. (a) The MARTINI CG sites and their labeling for (a) polyp and (b) the CG structure of polyP.

Table S6. The MARTINI CG bonded potentials and parameters for polyP and $(PEG)_{24}$-R_1.

Bead	Type	Functional form	Parameters
$BCE-BH_1$	Bond	$V_b(r_{ij})=\frac{1}{2}k_b(r_{ij}-b)^2$	$k_b=22000\frac{Kj}{mol.nm^2};b=0.27nm$
BH_1-BH_2	Bond	$V_b(r_{ij})=\frac{1}{2}k_b(r_{ij}-b)^2$	$k_b=8000\frac{Kj}{mol.nm^2};b=0.35nm$
BH_2-BH_3	Bond	$V_b(r_{ij})=\frac{1}{2}k_b(r_{ij}-b)^2$	$k_b=17000\frac{Kj}{mol.nm^2};b=0.39nm$
$BP-BP\ (SBP)$	Bond	$V_b(r_{ij})=\frac{1}{2}k_b(r_{ij}-b)^2$	$k_b=17000\frac{Kj}{mol.nm^2};b=0.27nm$
$BC-BCE-BH_1$	Angle	$V_a(\theta)=\frac{1}{2}k_\theta\frac{(\cos\theta-\cos\theta_0)^2}{\sin^2\theta}$	$k_\theta=20\frac{Kj}{mol};\theta_0=130^\circ$
$BCE-BH_1-BH_2$	Angle	$V_a(\theta)=\frac{1}{2}k_\theta\frac{(\cos\theta-\cos\theta_0)^2}{\sin^2\theta}$	$k_\theta=5\frac{Kj}{mol};\theta_0=45^\circ$
$BH_1-BH_2-BH_3$	Angle	$V_a(\theta)=\frac{1}{2}k_\theta\frac{(\cos\theta-\cos\theta_0)^2}{\sin^2\theta}$ *	$k_\theta=10\frac{Kj}{mol};\theta_0=86^\circ$
$BH_3-BH_2-BH_3$	Angle	$V_a(\theta)=\frac{1}{2}k_\theta(\cos\theta-\cos\theta_0)^2$	$k_\theta=65\frac{Kj}{mol};\theta_0=112^\circ$
$BP-BP(SBP)-BP(SBP)$	Angle	$V_a(\theta)=\frac{1}{2}k_\theta(\theta-\theta_0)^2$	$k_\theta=500\frac{Kj}{mol.rad^2};\theta_0=99^\circ$
$BC-BC-BCE-BH_1$	Dihedral	$V_d(\phi)=k_\phi(1+\cos(\phi-\phi_s))$	$k_\phi=3\frac{Kj}{mol};\phi_s=-100°$
$BC-BCE-BH_1-BH_2$	Dihedral	$V_d(\phi)=k_\phi(1+\cos(\phi-\phi_s))$	$k_\phi=6\frac{Kj}{mol};\phi_s=60°$
$BCE-BH_1-BH_2-BH_3$	Dihedral	$V_d(\phi)=k_\phi(1+\cos(\phi-\phi_s))$	$k_\phi=3\frac{Kj}{mol};\phi_s=50°$
$BP-BP-BP(SBP)-BP(SBP)$**	Dihedral	$V_d(\phi)=k_\phi(1+\cos(\phi-\phi_s))$	$k_\phi=4.5\frac{Kj}{mol};\phi_s=0°$

* Ref [20]

** The initial and terminal phosphate beads were not considered for the dihedral interactions.

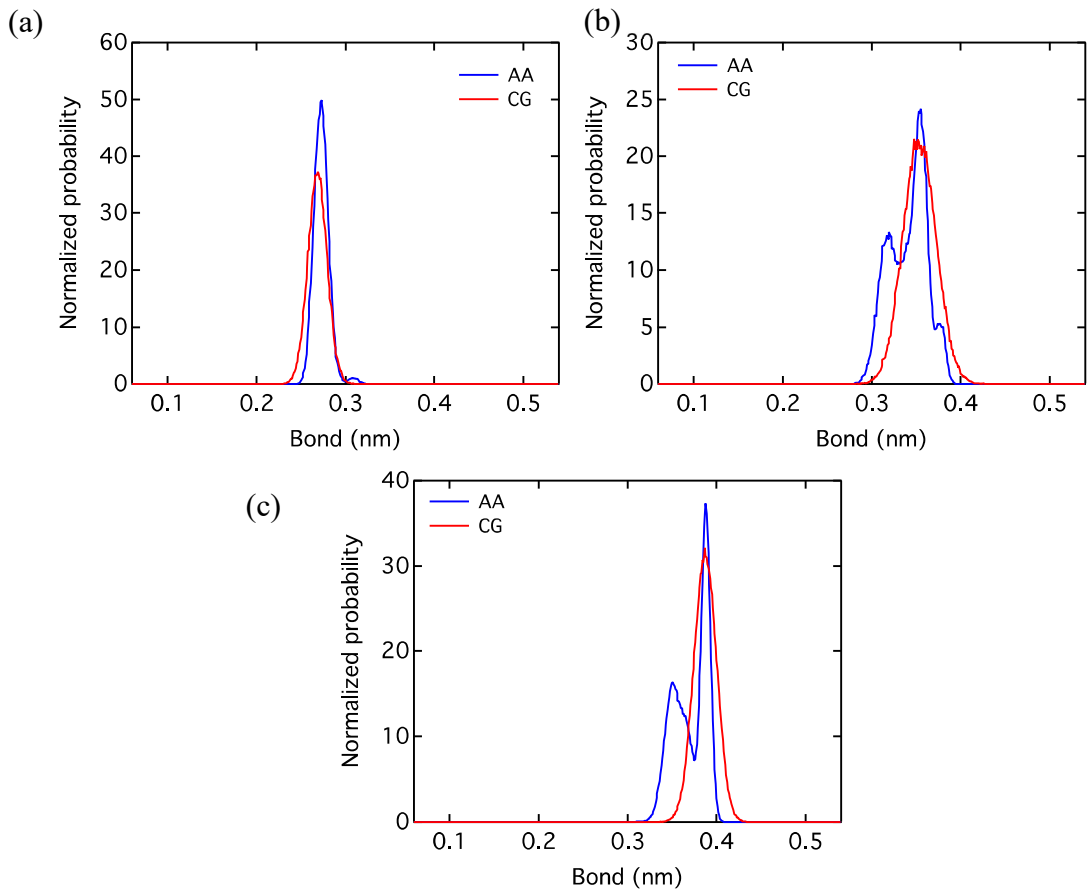

Figure S12. Bond stretching probability profiles for AA and CG for (a) $BCE - BH_1$, (b) $BH_1 - BH_2$, and (C) $BH_2 - BH_3$.

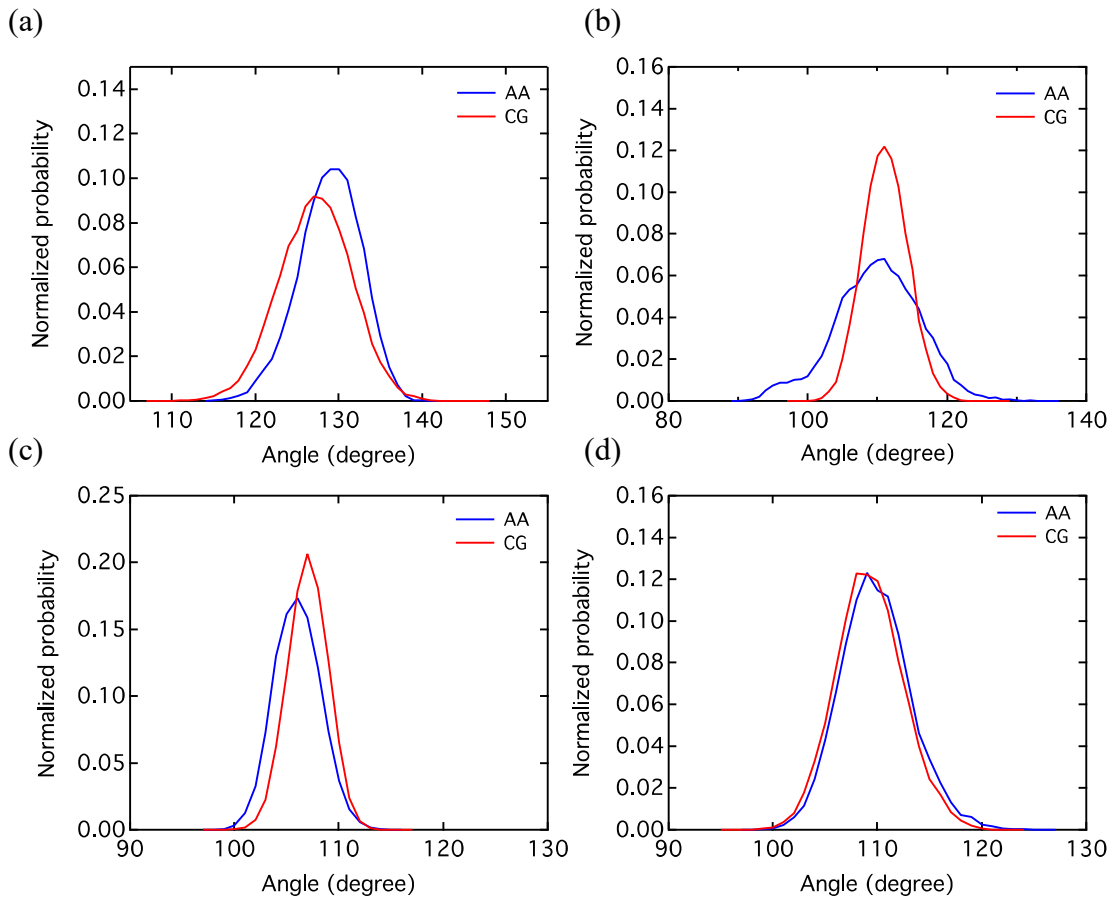

Figure S13. Angular bending probability profiles for AA and CG for (a) $BC - BCE - BH_1$, (b) $BCE - BH_1 - BH_2$, and (C) $BH_1 - BH_2 - BH_3$, and (d) $BH_3 - BH_2 - BH_3$.

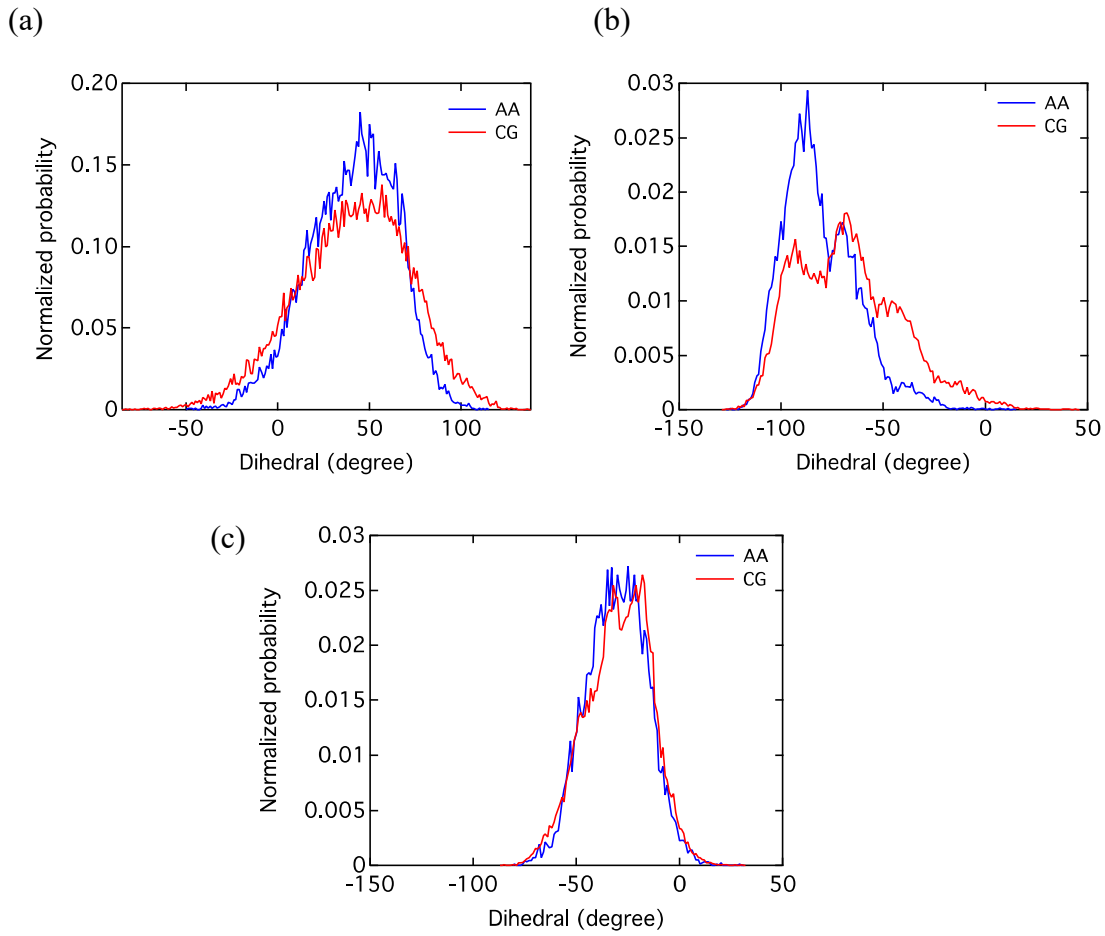

Figure S14. Torsional angle probability profiles for AA and CG for (a) $BC - BC - BCE - BH_1$, (b) $BC - BCE - BH_1 - BH_2$, and (C) $BCE - BH_1 - BH_2 - BH_3$.

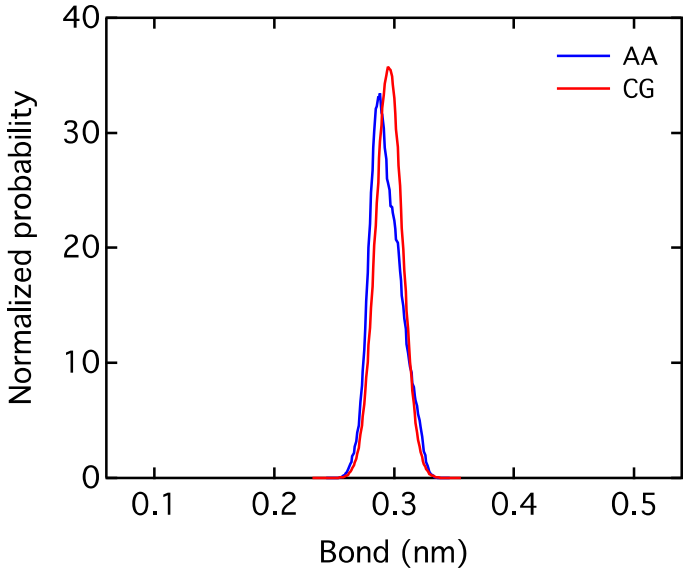

Figure S15. Bond stretching probability profiles for AA and CG for (a) $BP - BP$ (SBP)

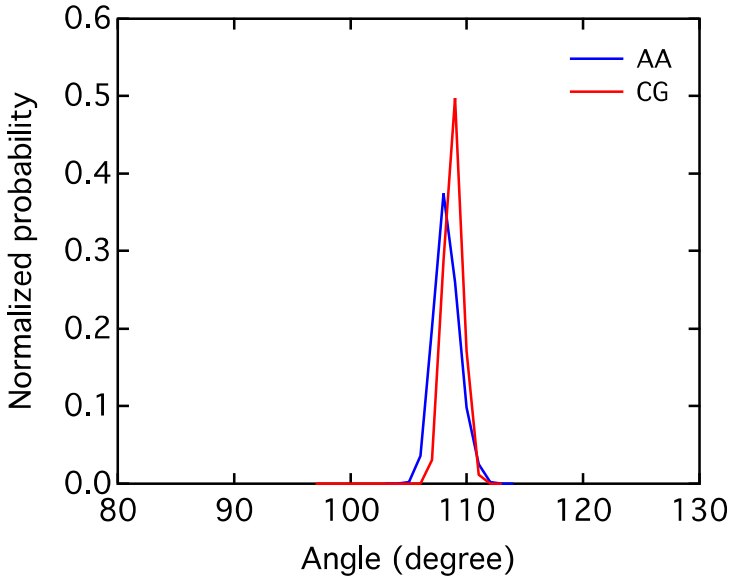

Figure S16. Angular bending probability profiles for AA and CG for (a) $BP -$

$BP(SBP) - BP(SBP)$.

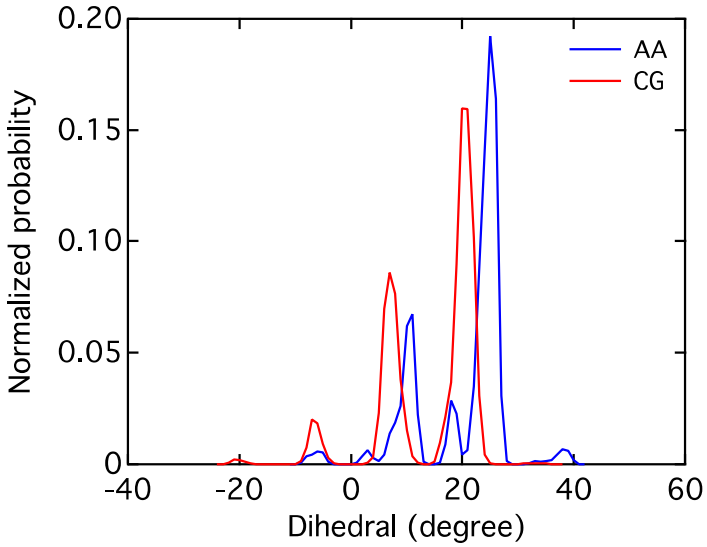

Figure S17. Torsional angle probability profiles for AA and CG for (a) $BP - BP - BP(SBP) - BP(SBP)$.

Table S7. The types and charges of MARTINI CG beads for polyP and $(PEG)_{24}$-R_1.

Bead	Type	Charge
BC	SN0	0
BCE	SP2	0
BH1	SQd	+1
BH2	N0	0
BH3	Qd	+1
BP	Qa	-1 (-2)*
SBP	SQa	-1

* The charge of initial and terminal BP (PO4-) is -2. The charge of the rest BP (PO3-) is -1.

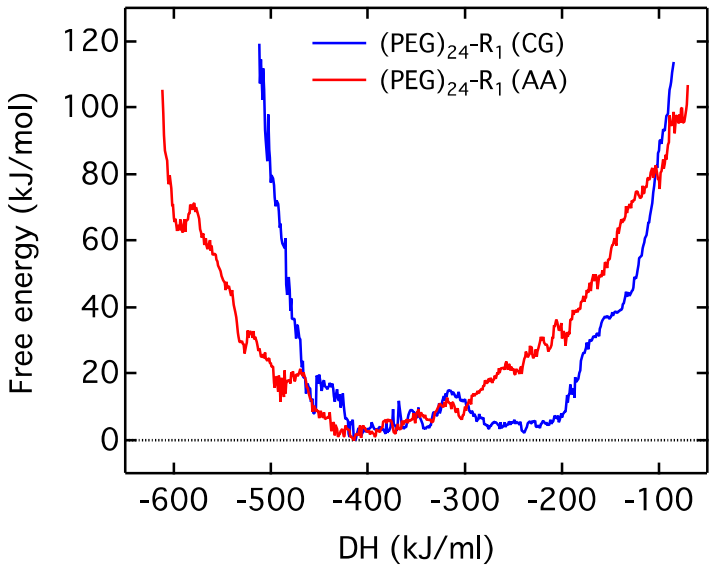

Figure S18. Free energy as a function of the DH energy.

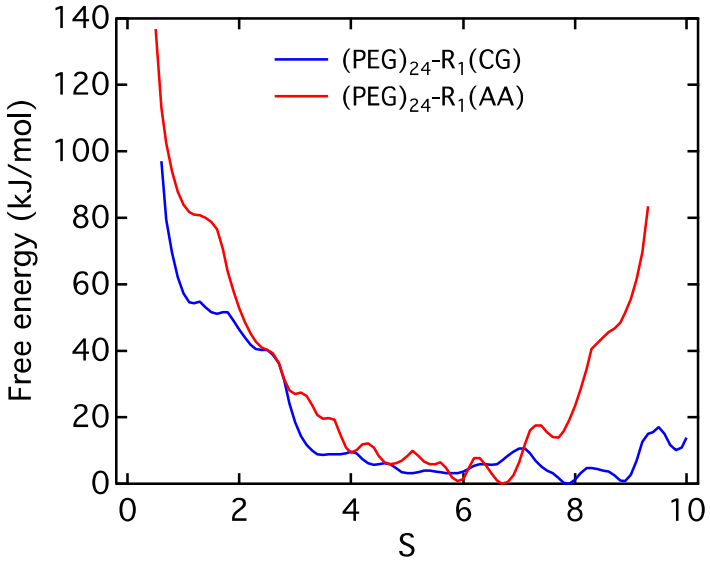

Figure S19. Free energy as a function of stoichiometry (S) number.

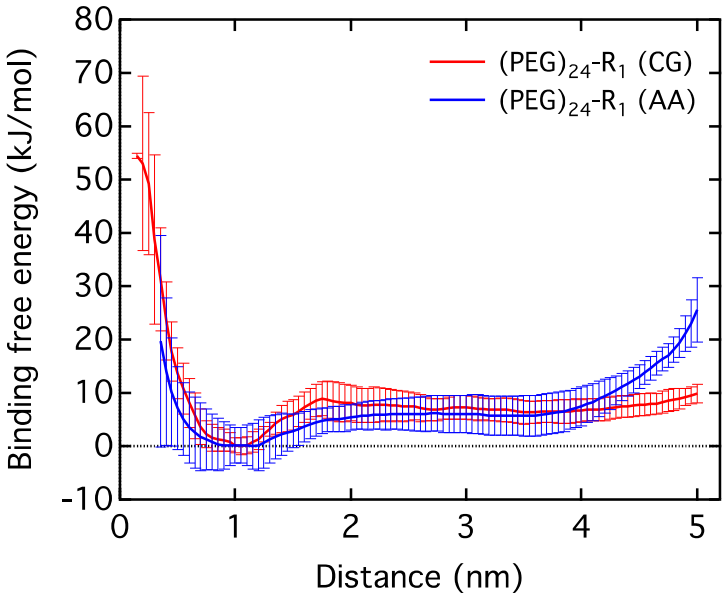

Figure S20. Binding free energy between the $(PEG)_{24}$-R_1 and polyP. The distance is defined between the polyP center of mass and the center of mass of drug headgroups.

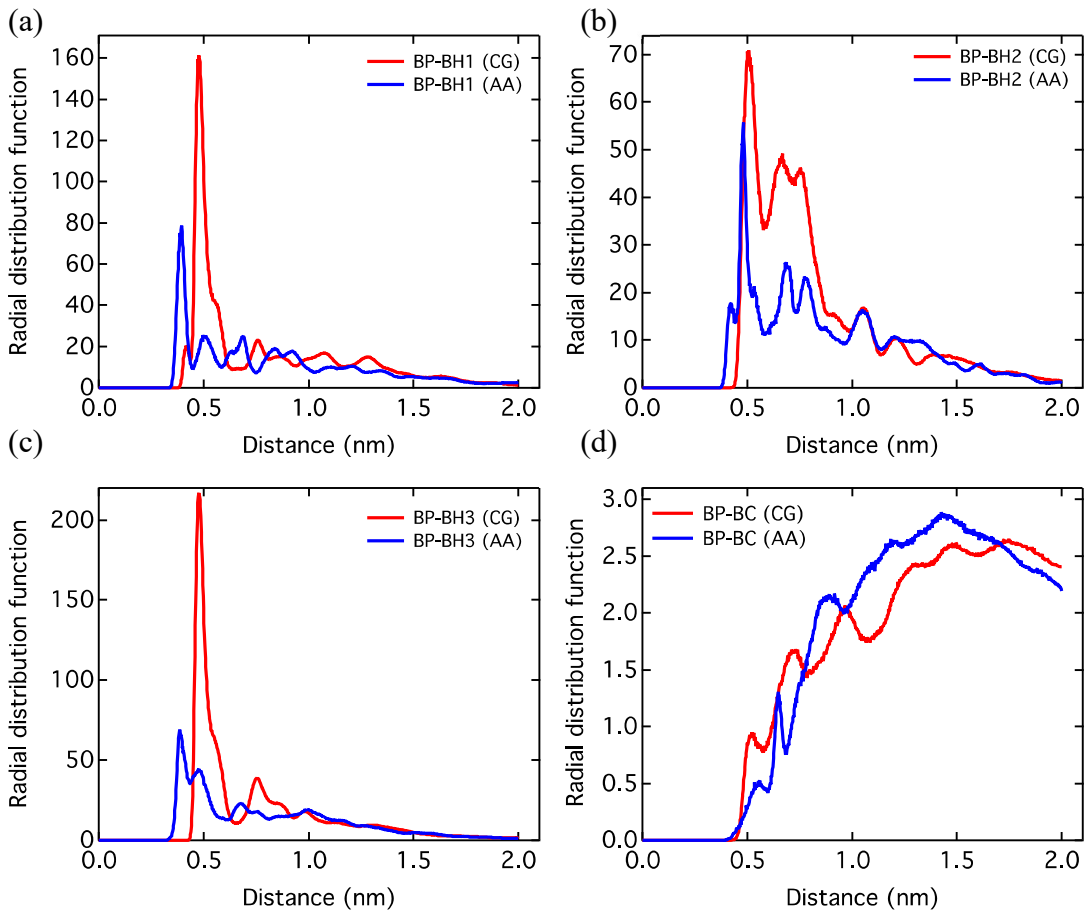

Figure S21. Radial distribution functions between BP (SBP) and (a) BH1, (b) BH2, (c) BH3, and (d) BC obtained by AA force field (blue) and CG force field (red) for system1. BP beads were the reference points in all calculations.

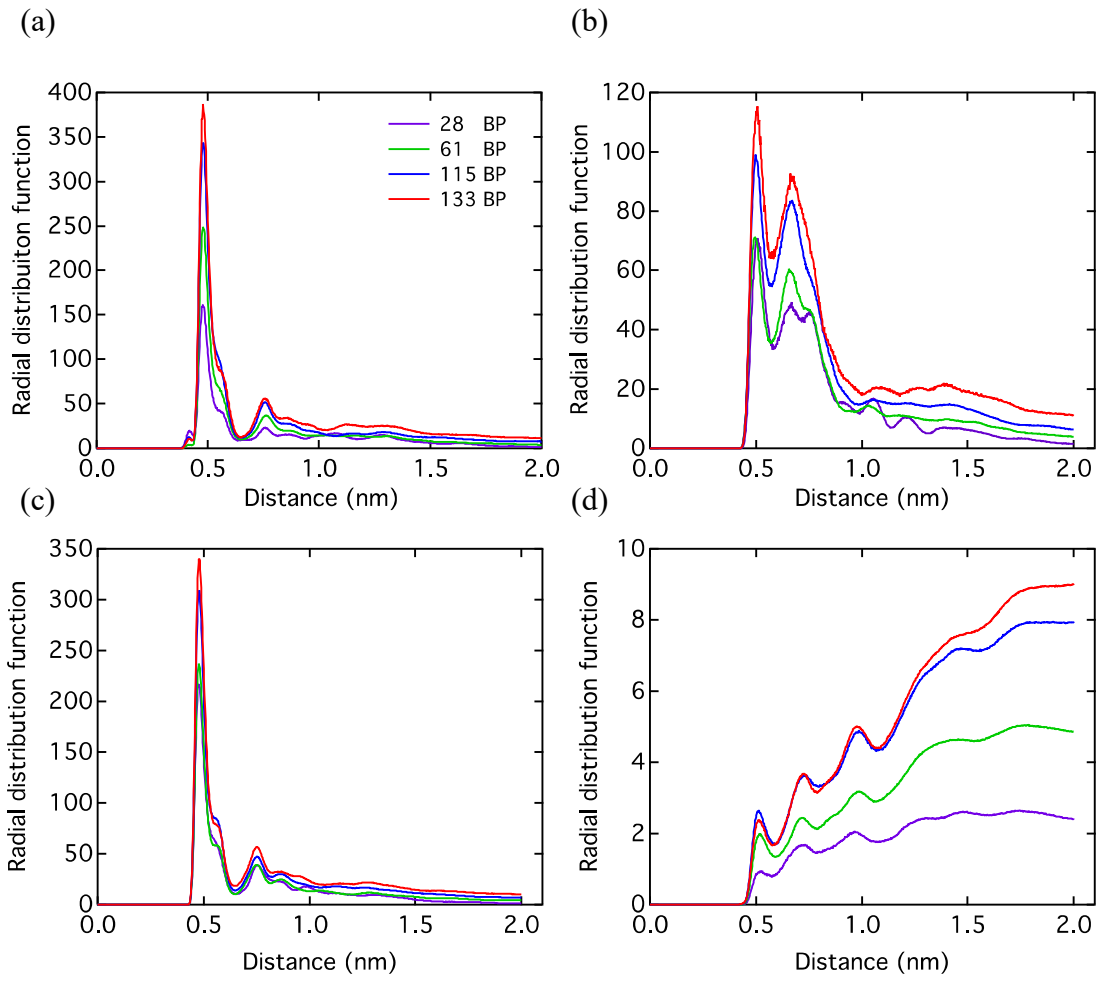

Figure S22. Radial distribution functions between BP (SBP) and (a) BH1, (b) BH2, (c) BH3, and (d) BC (BCE). BP beads were the reference points in all calculations.

Experimental Validation:

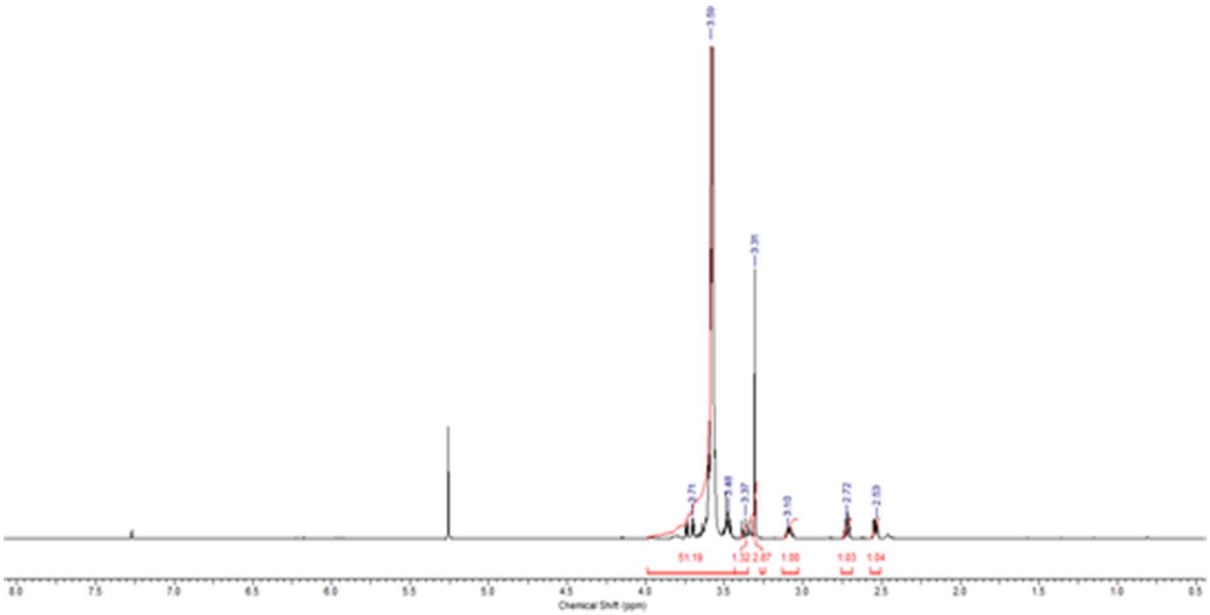

Figure S23: ^{1}H NMR spectrum of *m*-PEG550 epoxide

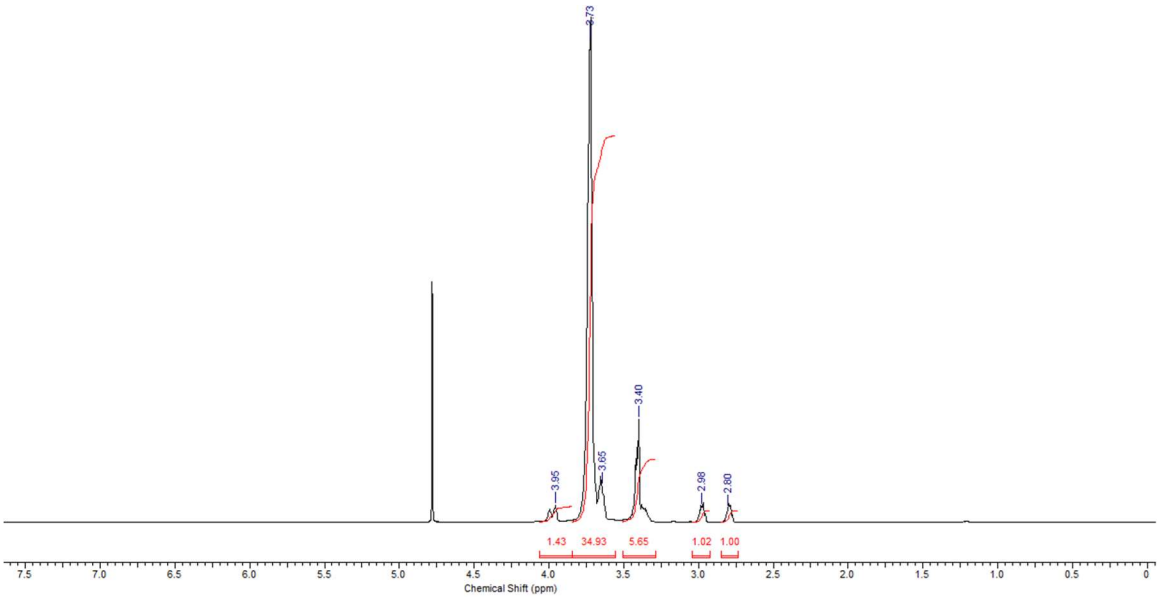

Figure S24: ^{1}H NMR spectrum of *m*-PEG350 epoxide

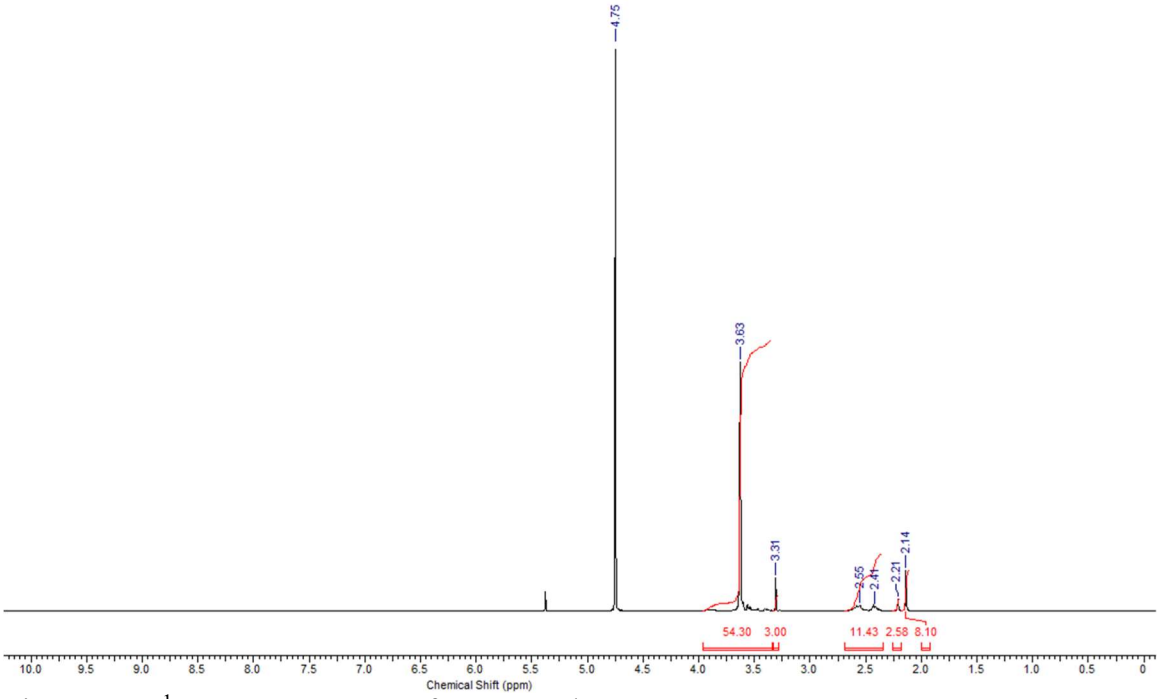

Figure S25: ^{1}H NMR spectrum of compound II

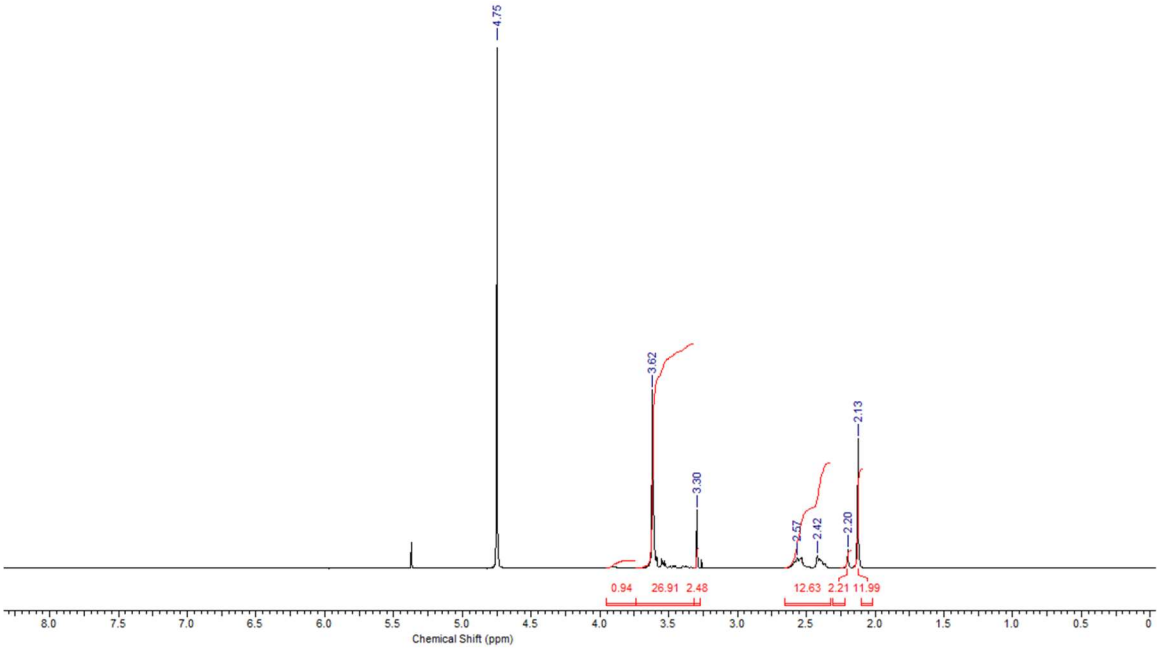

Figure S26: ^{1}H NMR spectrum of Compound III.

Reference

1. Marrink, S. J.; Tieleman, D. P., Perspective on the Martini Model. *Chem. Soc. Rev.* **2013**, *42*, 6801-6822.
2. Wang, J.; Wolf, R. M.; Caldwell, J. W.; Kollman, P. A.; Case, D. A., Development and Testing of a General Amber Force Field. *J. Comput. Chem.* **2004**, *25*, 1157-74.
3. Http://Cgmartini.Nl/Images/Parameters/Itp/Martini_V2.2p.Itp.
4. Yesylevskyy, S. O.; Schafer, L. V.; Sengupta, D.; Marrink, S. J., Polarizable Water Model for the Coarse-Grained Martini Force Field. *Plos Comput. Biol.* **2010**, *6*.
5. Sugita, Y.; Okamoto, Y., Replica-Exchange Molecular Dynamics Method for Protein Folding. *Chem. Phys. Lett.* **1999**, *314*, 141-151.
6. Barducci, A.; Bussi, G.; Parrinello, M., Well-Tempered Metadynamics: A Smoothly Converging and Tunable Free-Energy Method. *Phys. Rev. Lett.* **2008**, *100*, 020603.
7. Bonomi, M.; Parrinello, M., Enhanced Sampling in the Well-Tempered Ensemble. *Phys. Rev. Lett.* **2010**, *104*, , 190601.
8. Bussi, G.; Gervasio, F. L.; Laio, A.; Parrinello, M., Free-Energy Landscape for Beta Hairpin Folding from Combined Parallel Tempering and Metadynamics. *J. Am. Chem. Soc.* **2006**, *128*, 13435-13441.
9. Hess, B., P-Lincs: A Parallel Linear Constraint Solver for Molecular Simulation. *J. Chem. Theory Comput.* **2008**, *4*, 116-122.
10. Pronk, S., et al., Gromacs 4.5: A High-Throughput and Highly Parallel Open Source Molecular Simulation Toolkit. *Bioinformatics* **2013**, *29*, 845-854.

11. Abraham, M. J.; Murtola, T.; Schulz, R.; Páll, S.; Smith, J. C.; Hess, B.; Lindahl, E., Gromacs: High Performance Molecular Simulations through Multi-Level Parallelism from Laptops to Supercomputers. *SoftwareX* **2015**, *1–2*, 19-25.
12. http://cgmartini.nl/images/parameters/exampleMDP/martini_v2.x_new.mdp.
13. Bussi, G.; Donadio, D.; Parrinello, M., Canonical Sampling through Velocity Rescaling. *J. Chem. Phys.* **2007**, *126*.
14. Parrinello, M.; Rahman, A., Polymorphic Transitions in Single-Crystals - a New Molecular-Dynamics Method. *J. Appl. Phys.* **1981**, *52*, 7182-7190.
15. Prakash, M. K.; Barducci, A.; Parrinello, M., Replica Temperatures for Uniform Exchange and Efficient Roundtrip Times in Explicit Solvent Parallel Tempering Simulations. *J. Chem. Theory Comput.* **2011**, *7*, 2025-2027.
16. Deighan, M.; Bonomi, M.; Pfaendtner, J., Efficient Simulation of Explicitly Solvated Proteins in the Well-Tempered Ensemble. *J. Chem. Theory Comput.* **2012**, *8*, 2189-2192.
17. Tribello, G. A.; Bonomi, M.; Branduardi, D.; Camilloni, C.; Bussi, G., Plumed 2: New Feathers for an Old Bird. *Comput. Phys. Commun.* **2014**, *185*, 604-613.
18. Do, T. N.; Carloni, P.; Varani, G.; Bussi, G., Rna/Peptide Binding Driven by Electrostatics-Insight from Bidirectional Pulling Simulations. *J. Chem. Theory Comput.* **2013**, *9*, 1720-1730.
19. Tiwary, P.; Parrinello, M., A Time-Independent Free Energy Estimator for Metadynamics. *J. Phys. Chem. B* **2015**, *119*, 736-742.

20. Bulacu, M.; Goga, N.; Zhao, W.; Rossi, G.; Monticelli, L.; Periole, X.; Tieleman, D. P.; Marrink, S. J., Improved Angle Potentials for Coarse-Grained Molecular Dynamics Simulations. *J. Chem. Theory Comput.* **2013**, *9*, 3282-92.